Characteristics of seismic wave attenuation in the Kishtwar and its adjoining region of NW Himalaya

Anup K. Sutar (ID) **· Mithila Verma ·**
Brijesh. K. Bansal · G. M. Bhat · Shiv J. Pandey

Abstract We investigate the attenuation characteristics of high frequency seismic waves in the Kishtwar and its adjoining region of NW Himalaya using 161 local earthquakes (M 2.1–5.7), recorded by a local network of seven Broad Band Seismic (BBS) stations. The extended coda normalization technique and the single backscattering method are used to study the attenuation characteristics of body and coda waves, respectively. The study shows that the attenuation quality factors for P-wave (Q_α), S-wave (Q_β) and Coda wave (Q_c) are strongly dependent on frequency and increase with the increase in central frequency. The average frequency-dependent relationship for Q_α, Q_β and Q_c is found to be as $Q_\alpha = (44 \pm 7)f^{(1..01 \pm 0.91)}$, $Q_\beta = (71 \pm 6)f^{(0.91 \pm 0.01)}$ and $Q_c = (60 \pm 4)f^{(1.06 \pm 0.04)}$. The sites located on the western part of the study area exhibit higher attenuation (Q) compared with those in eastern part, suggesting that the eastern part of the study area is more heterogeneous than the western part. Variation of Q_c with increasing lapse time suggests that the lower lithosphere is less heterogeneous, compared with the upper crust. We infer that the heterogeneity in the upper crust of Kishtwar area is primarily, due to the presence of highly fractured strata, dense network of joints and local faults, which mainly include splays of regional faults.

1 Introduction

Knowledge of attenuation characteristics of a region is essential for various seismological studies like simulation of synthetic accelerograms/seismograms, estimation of source parameters and developing shake models etc. The seismic wave energy gets attenuated when it travels through a medium, leading to decay in seismic wave amplitude. The attenuation of the seismic wave energy is mainly caused by anelasticity, geometrical spreading, scattering, reflection and transmission at the boundary (Stein and Wysession 2003). A dimensionless quantity, known as the quality factor, Q is widely used to express the attenuation characteristics of the medium. It characterizes the energy loss per unit

A. K. Sutar (✉)
Ministry of Earth Sciences, Borehole Geophysics Research Laboratory, Karad, India
e-mail: anupseismo@gmail.com

M. Verma · B. K. Bansal
Geoscience/Seismology Division, Ministry of Earth Sciences, New Delhi, India

G. M. Bhat · S. J. Pandey
University of Jammu, Jammu, India

oscillation cycle and attenuation is inversely pro-portional to Q (Knopoff 1964). Thus, Q is directly related with the medium properties, and study of this parameter significantly characterizes the diver-sity of physical properties of the earth and seismic potential of any given region (Singh and Herrmann 1983). The quality factor Q has been widely esti-mated using P-wave, S-wave, coda-wave and Lg-wave (Aki 1969; Yoshimoto et al. 1993; Mitchell 1995) commonly referred to as, Q_α,Q_β, Q_c and Q_{Lg} respectively.

The study of coda waves attenuation is useful in understanding the average attenuation properties of the medium, whereas the body waves and surface waves could provide the attenuation only along their direct paths, either between the receiver and the sta-tion or between the two stations. The coda waves are considered as the superposition of backscattered waves, which are generated by strong heterogenei-ties distributed randomly in the crust and the upper mantle (Aki 1969; Aki and Chouet 1975; Rautian and Khalturin 1978). The heterogeneity in the crust is mainly produced by complex geological subsurface structures, irregular topography, faults, cracks and the heterogeneous elastic properties of the rock. Thus, the coda waves provide an average attenuation of the whole medium and are useful in retrieving informa-tion from a few meters to several kms in the upper crust.

Kishtwar region lies in Kashmir seismic gap of NW Himalaya and being adjacent to active Chamba seismic zone, it is also seismically active. However, it is observed that even being seismically active, the region has not been studied in terms of seismic attenuation. In the present study, we estimated the seismic waves attenuation characteristics of Kishtwar region for the first time to get insights on the struc-tural heterogeneity beneath the region and its relation to seismicity of the area. The coda attenuation has been estimated using the single back-scattering model (Aki 1969), whereas P- and S- wave attenuation is estimated by the extended coda normalization method (Yoshimoto et al. 1993). These results provide new light in understanding the seismotectonic setting of the NW Himalaya and the estimated attenuation parameters will be useful in strong ground motion simulation, source parameter studies and hazard esti-mation for the region, which are earlier unknown for the study area.

2 Geo-tectonic set up and seismicity

The study area lies in Kashmir Himalaya, a part of northwest Himalayan collision zone in the Indian subcontinent. Due to its proximity to the western syntaxial bend, Kashmir Himalaya is tectonically active and has witnessed several devastating earth-quakes in the past. The Western Syntaxis is charac-terised by rock formations with fold belts and thrust systems and abruptly bend southwards making acute knee like bend. Kashmir Himalaya includes Hazara syntaxis, where the rock formations of Pir Panjal Range are severely folded and split repeat-edly by the thrusts along the axis of the folds (Valdiya 2016). The region is traversed by north-east dipping major intracrustal thrusts from south to north; the Main Boundary Thrust (MBT), Main Central Thrust (MCT) and Southern Tibet Detach-ment (STD) and the Indus Tsangpo Suture Zone (ITSZ) which divide the region into major geologi-cal belts namely, Lesser Himalaya, Higher Hima-laya Crystalline (HHC), Tethys Himalaya Sequence (THS) and the Trans-Himalaya / Ladakh Batholith. The region is also exposed to many local faults and thrusts mostly the splays of major NW–SE trending faults/thrusts. The Kishtwar Fault to the west and Sundarnagar Fault to the east of study area are the local transverse faults, which control the seismicity in west and east, respectively (Fig. 1).

A part of Kashmir Himalaya, comprising Chamba, Kishtwar and Zanskar regions, is char-acterised by a unique geological setup where the Tethys Himalayan rocks lie in contact with the Lesser Himalayan thrust and the Higher Himala-yan Crystallines (HHC). The area where Lesser Himalayan imbricated sequence, extended deep beneath the crust, crops-out within the Higher Him-alayan Crystallines is referred as Kishtwar Window (Fig. 1) which is bounded by MCT in the north-east and Kishtwar thrust in the south. The area is also characterised by the presence of main litho-structural units, thrusted and transported south-ward named as Kashmir Nappe and Chamba Nappe. Kashmir Nappe zone constitutes of palaeozoic-Mesozoic marine sediments with Precambrian base-ment and thrusted along Pir-Panjal thrust, a regional tectonic plane (Wadia 1931). The Chamba Nappe is characterised by weakly metamorphosed Tethys
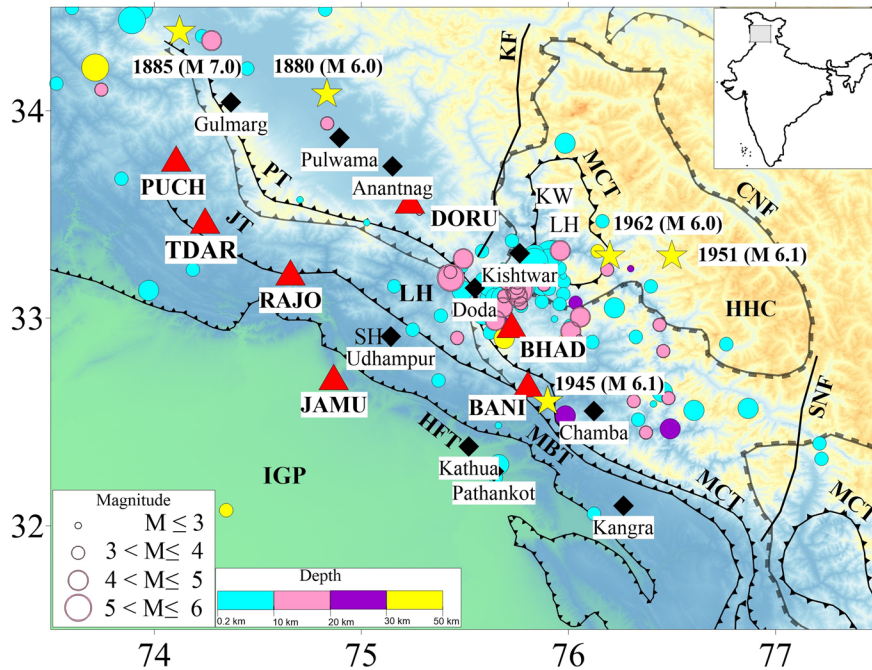
Fig. 1 Tectonic map of J&K region, projected over the topographic map. The abbreviations used are HFT (Himalayan Frontal Thrust), MBT (Main Boundary Thrust), MCT (Main Central Thrust), CNF (Chenab Normal Fault), (PT) Panjal Thrust, JT (Jammu Thrust), IGP (Indo Gangetic Plains), SH (Sub Himalaya), LH (Lesser Himalaya), HHC (Higher Himalayan Crystalline), KW (Kishtwar Window). KF (Kishtwar Fault), SNF (Sundarnagar fault). Red triangles represent Broad Band Seismic (BBS) stations, and black diamonds represent important cities around the study region. Circles with increasing diameters are earthquakes recorded by the BBS networks between Jan 2013 and Oct 2016. The colour of the circles represents depth distribution of events. The colour scale for the depth range and the corresponding diameter for the magnitude of events is given in the legend section. Important historical events are also superimposed over the map using yellow stars and labelled

Himalayan Sequence thrusted from the north over the metamorphic Higher Himalayan Crystellines (Thakur 1992).

The region is continuously under stress due to NE thrusting of Indian plate under Eurasia plate and its proximity to western syntaxis. Many destructive earthquakes have visited the region, like 1885 Kashmir earthquake (M7.0) with the epicentre just north of the Wular Lake and 2005 Kashmir earthquake (Mw 7.6). Nearly 3200 people were reported killed in J&K region during 1885 earthquake, while more than 80,000 lost their lives in 2005 earthquake. In addition, many small and moderate earthquakes have occurred in this region. A spurt of earthquake events occurred in Kishtwar region during May to August 2013 with the largest earthquake of magnitude Mw 5.7 (Pandey et al. 2016) and the seismic activity continues in the area. Several moderate earthquakes have occurred in the region since May 2013, which includes 7 earthquakes of M > 5 and 55 events of 5 > M > 4.

3 Methodology

We used single scattering model for estimation of coda wave attenuation Aki (1969). Different lapse time windows are analysed to examine the multiple scattering effects (Peng et al. 1987). For estimation of body wave attenuation properties, extended coda-normalization method given by Yoshimoto et al. (1993) is used in the study.

3.1 Coda attenuation study

The backscattering model of Aki (1969) makes an estimation of the total Q i.e. Q_c, which depends on both scattering and intrinsic properties of the

attenuation. The observed amplitude of the coda wave can be modelled using the following relationship (Aki and Chouet 1975)

$$A(f,t) = S(f)t^{-m}e^{-\pi ft/Q_c(f)} \tag{1}$$

where A(*f, t*) is the spectral amplitude observed at lapse time 't' and frequency *f*, S(*f*) is the source term, 'm' is the geometrical spreading term and m = 1 for body waves, as coda waves are back scattered body waves (Sato and Fehler, 1998).

Taking the natural logarithm of Eq. (1) and arranging the terms, we get the following equation,

$$\ln(A(f,t).t) = \ln(S(f)) - \pi ft/Q_c(f) \tag{2}$$

By performing a linear regression between $ln(A(f,t).t)$ versus time *t*, Q_c can be obtained from the slope of the regressed line. The source term has no influence on the slope, and the start time of the coda window is assumed to be twice the travel time of S-wave arrival. The frequency-dependent Q_c can be obtained approximately using the formula given by Rautian and Khalturin (1978).

$$Q_c = Q_0 f^n \tag{3}$$

where *n* is called frequency exponent parameter and Q_0 is the value of quality factor at 1 Hz. Taking natural logarithm on both the sides of Eq. (3), we arrive at the following,

$$\text{In}(Q_c) = \text{In}(Q_0) + n\,\text{In}(f) \tag{4}$$

Here, Q_0 can be determined from the linear regression between $\ln(Q_c)$ and $\ln(f)$.

3.2 P- and S-wave attenuation

The extended coda-normalization method (Yoshimoto et al. 1993) is used to estimate the attenuation properties of the body waves. The method assumes that the coda wave energy is homogeneously distributed near the source. In this method the spectral amplitudes of direct P-wave (A_α) and S-wave (A_β) are divided by the coda spectral amplitude (A_c) to remove the effects of source excitation, site amplification and instrument response. The method enables estimation of Q_α and Q_β by normalizing the direct P- and S-wave spectral amplitude (A_α and A_β) by the coda-spectral amplitude (A_c) measured at a fixed

lapse time, roughly greater than twice the direct S-wave travel time measured from the earthquake origin time.

The spectral amplitude, $A_c(f,t_c)$ of the coda wave at a particular lapse time, *tc* can be written as:

$$A_c(f,t_c) = S(f)P(f,t_c)G(f)I(f) \tag{5}$$

where *f* is the frequency, S (*f*) is the source term and $P(f,t_c)$ is the coda excitation term, which represents the decay of spectral amplitude of coda waves with lapse time. G(*f*) is the site amplification factor and I(*f*) is the instrumental response. The spectral amplitude of the direct P wave, $A_\alpha(f,r)$, can be written as

$$A_\alpha(f,r) = R_{\theta\varphi}S(f)r^{-a}exp\left(\frac{-\pi fr}{Q_\alpha(f)V_\alpha}\right)G(f,\Psi)I(f) \tag{6}$$

where $R_{\theta\varphi}$ is the source radiation pattern, S(*f*) represents the source term, *r* is the distance from the source, *a* represents the geometrical spreading, $Q_\alpha(f)$ is the P-wave quality factor, V_α is the average P-wave velocity and $G(f,\Psi)$ is the site amplification term, where Ψ is the incident angle of P-waves and I(*f*) is the instrument correction term. Dividing Eq. (6) by (5), it can be obtained as:

$$\frac{A_a(f,r)}{A_c(f,t_c)} = R_{\theta\varphi}\,r^{-a}\,\frac{G(f,\psi)}{G(f)}\,P^{-1}\,(f,t_c)\,exp\left(\frac{-\pi fr}{Q_a(f)\,V_a}\right) \tag{7}$$

For a fixed t_c, the value of $P^{-1}(f,t_c)$ is only a function of *f* and can be written as Constant (*f*). Thus, taking logarithm of Eq. (7), it can be written as:

$$ln\left(\frac{R_{\theta\varphi}^{-1}A_\alpha(f,r)r^a}{A_c(f,t_c)}\right) = -\frac{\pi fr}{Q_\alpha(f)V_\alpha} + \ln\left(\frac{G(f,\psi)}{G(f)}\right) + const(f) \tag{8}$$

To determine the attenuation of P-wave quality factor (Q_a), Yoshimoto et al. (1993) assumed that the contribution of $R_{\theta\varphi}$ will disappears over many different types of faulting mechanism. Similarly, $G(f,\psi)/G(f)$ is independent of ψ over many events with various epicentral distances and becomes a variable of *f* only like $P^{-1}(f,t_c)$. Additionally, in the geometrical spreading factor r^a, where 'a' is assumed to be 1 for body waves. Considering the above assumptions, Eq. (8) can be written as:

$$ln\left(\frac{A_\alpha(f,r)r}{A_c(f,t_c)}\right)_{r\pm\Delta r} = -\frac{\pi fr}{Q_\alpha(f)V_\alpha} + const(f) \qquad (9)$$

such equation for the S-wave can also be obtained using the similar methodology

$$ln\left(\frac{A_\beta(f,r)r}{A_c(f,t_c)}\right)_{r\pm\Delta r} = -\frac{\pi fr}{Q_\beta(f)V_\beta} + const(f) \qquad (10)$$

The slope of the regression lines plotted between the left-hand side of equation Eqs. 9 and 10 w.r.t. hypocentral distance is used to estimate the quality factors for P and S waves.

4 Data and analysis

A seismic network consisting of seven Broad Band Seismic (BBS) stations in the study region at the remote locations, namely, Bani, Poonch, Doru, Jammu, Rajouri, Bhaderwah and Tangdhar (Table 1), is running since 2009. Each station is equipped with a Trillium 240 seismometer coupled with Taurus digitizer and the data are collected at a rate of 100 samples per second. Data recorded by the network between 2013 and 2016 are used in the present study. The seismicity plot (Fig. 1) shows that most of the events are concentrated within MBT and KW with a few events falling near the remote sites, such as Poonch and Tangdhar areas. During this monitoring period, 161 events were recorded at least at three seismic stations (Fig. 1). The events were processed using the SEISAN software package developed by Havskov & Ottemöller (2010) and located using the velocity model of Kumar et al. (2009). The root mean square (RMS) error between observed and theoretical travel time difference of the located events varies between

0.1 and 1.8 s, while the magnitude and depth of the located events vary between M 2.1–5.7 and 0–40 km, respectively, with most of the events (~75%) exhibiting shallower depth < 10 km (Fig. 1).

4.1 Coda wave attenuation (Q_c)

The 'CODAQ' subroutine (Havskov & Ottemöller 2010) is used for estimating Q_c. Only the waveforms having a good signal-to-noise ratio (S/N ≥ 2) are used for analysis. S/N ratios are calculated for each central frequency for every record. We estimated S/N ratio by considering the RMS amplitude of the last 5-s lapse time window, which is divided by the seismic noise data of the equal length before the arrival of P-wave. Similarly, the criterion for correlation coefficient of ≥ 0.50 is applied to obtain reliable Q_c values. Havskov and Ottemöller (2010) suggest that the coda window length should be a minimum of 20 s to get stable results, and there is no limit on choosing the maximum lapse time. However, S/N ratio ≥ 2 could not be obtained for lapse time > 60 s for many events; hence, we chose 60 s to be the upper limit in our study. Three lapse time windows with duration 40, 50 and 60 s are considered, and the coda window length is fixed to be 20 s. Figure 2 shows an example of a selected coda window length used in the analysis.

A Butterworth bandpass filter is applied on the selected window at central frequencies of 1.5, 2.0, 4.0, 6.0 and 12.0 Hz and linear regression is performed between $ln[A(f,t).t]$ versus t (Fig. 2). The slope (s) of the regressed line is used to estimate Q_c. Table 2 lists the estimated Q_c at each station, and Fig. 3 provides the plots for estimated Q_0 at each station and average Q_0 in the study region. Table 3 provides details of the average Qc at different lapse times and central frequencies and the average value of power-law Q_0f^n at different lapse time and different

Table 1 Location coordinates of Broadband Seismic (BBS) stations

Sl No	Station name	Station code	Latitude (^{0}N)	Longitude (^{0}E)	Elevation (m)
1	Jammu	JAMU	32.718	74.867	350
2	Bani	BANI	32.684	75.804	1393
3	Doru	DORU	33.567	75.234	1833
4	Tangdhar	TDAR	33.470	74.246	1852
5	Rajouri	RAJO	33.221	74.657	1111
6	Poonch	PUCH	33.770	74.106	1054
7	Bhaderwah	BHAD	32.967	75.726	1700
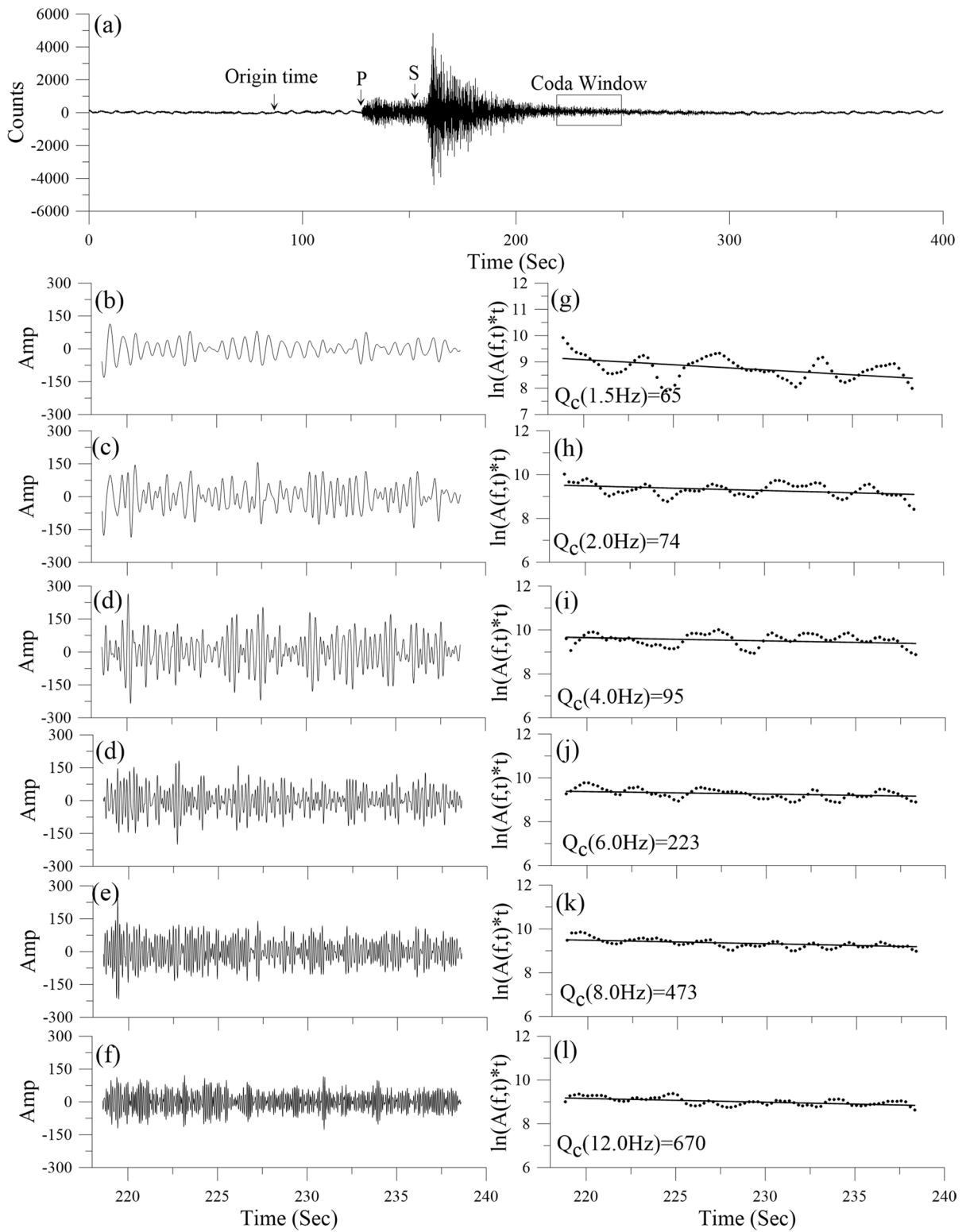
◄**Fig. 2** (**a**) A selected event is marked for the origin time, P and S onsets along with the coda widow to estimate the coda Q (Q_c). (**b** to **f**) shows the filtered coda window at different frequencies. (**g–l**) shows the regression of the coda window and the fit to estimate coda Q_c for individual frequencies. The estimated coda Q_c is also marked in the lower corner of the figure

central frequencies for each station are given in Table 4. Figure 4 depicts the variation of Q_c at different lapse time at each station and estimation of $Q_o f^n$ for each lapse time variation.

In the single scattering model, coda waves are considered as the average back-scattered waves on the ellipsoid volume having the station and the source as focus (Pulli 1984). Using this approximation, the ellipsoidal volume for each seismic station is estimated. The estimated Q_c reflects the average attenuation properties of the ellipsoidal volume with an average depth, $h = h_{av} + a_2$, where (i) h_{av} is the average focal depth of the events and (ii) $a_2 = \sqrt{a1^2 - \Delta^2}$ is the semi-minor axis of the ellipsoidal volume (Pulli 1984) and Δ is the average epicentral distance. The semi-major axis of the ellipsoidal volume is assumed to be $a_1 = ct/2$, where t is the average lapse time and c is the velocity of S wave ($c = 3.5$ km/s). The average lapse time is estimated as $t = t_{start} + W/2$, where t_{start} is the starting time of the coda waves and W is the coda window length. The calculated depths for the ellipsoidal volume for different stations are given in Table 5.

4.2 Attenuation of P and S-wave (Q_α and Q_β)

For the estimation of P- and S-wave quality factors, we developed a MATLAB code. The code takes input from the SEISAN S-files on the location, origin time and P- and S-wave arrival times. A 2.5-s window is selected after the onset of P- and S-waves, and 30-s window is selected after the Coda arrivals. A 2.5-s noise window is also selected before the onset of P-wave to estimate the SNR. The RMS amplitudes of P and S waves are normalized by the selected coda waves and a graph is plotted between $ln\left(\frac{A_{\beta,\alpha}(f,r)r}{A_c(f,t_c)}\right)$ vs hypocentral distance (r). The slope of the best-fitted lines is used to estimate the quality factors for the P- and S-waves following Eqs. 9 and 10, respectively. The average velocity of P- and S-waves has been taken as 6.1 and 3.5 km/s of P- and S-waves respectively following Kumar et al. (2009). An example of the estimated Q_α and Q_β for the BANI station is shown in Fig. 5, and details of the estimated Q_α and Q_β for each station are given in Table 6. The variation of power-law $Q_o f^n$ at each station for Q_α, Q_β and Q_c is given in Table 7, and the power-law for Q_α and Q_β at each station is plotted in Fig. 6. The average values of Q_α, Q_β and Q_c at each central frequency are plotted in (Fig. 7).

5 Results and discussion

We estimated the quality factors Q_α, Q_β and Q_c for the Kistwar and adjoining areas at six central frequencies, i.e. 1.5, 2.0, 4.0, 6.0, 8.0 and 12 Hz for each station to understand the attenuation properties of the study region vis-a-vis their implication to the structural heterogeneity and seismotectonic. We observed that the Q_α, Q_β and Q_c increase with increasing central frequencies (Tables 2 and 6) and the frequency-dependent relation $Q = Q_0 f^n$ for each station (Table 7) shows that Q_α varies between $(28 \pm 2) f^{(0.86 \pm 0.08)}$ at

Table 2 Variation of coda Q_c at different frequency band at different stations

Station code	1.5 (Hz)	2(Hz)	4(Hz)	6(Hz)	8(Hz)	12(Hz)	*$Q_c = Q_o f^n$
BANI	87 ± 4	119 ± 5	247 ± 12	379 ± 19	513 ± 25	788 ± 39	$62 \pm 4 f^{1.06 \pm 0.04}$
BHAD	85 ± 4	115 ± 5	245 ± 12	380 ± 19	519 ± 26	806 ± 40	$61 \pm 4 f^{1.08 \pm 0.04}$
DORU	90 ± 7	122 ± 9	258 ± 20	399 ± 32	544 ± 43	843 ± 67	$65 \pm 6 f^{1.08 \pm 0.06}$
JAMU	91 ± 4	124 ± 5	264 ± 12	410 ± 18	560 ± 25	871 ± 39	$65 \pm 5 f^{1.09 \pm 0.05}$
PUCH	94 ± 3	129 ± 5	271 ± 11	419 ± 17	571 ± 23	882 ± 36	$67 \pm 5 f^{1.07 \pm 0.03}$
RAJO	101 ± 7	138 ± 10	293 ± 22	455 ± 34	621 ± 47	964 ± 73	$74 \pm 9 f^{1.09 \pm 0.06}$
TDAR	93 ± 3	123 ± 5	245 ± 10	366 ± 15	486 ± 20	726 ± 30	$60 \pm 4 f^{0.99 \pm 0.03}$

*Coda start time is taken as twice the travel time of S-wave
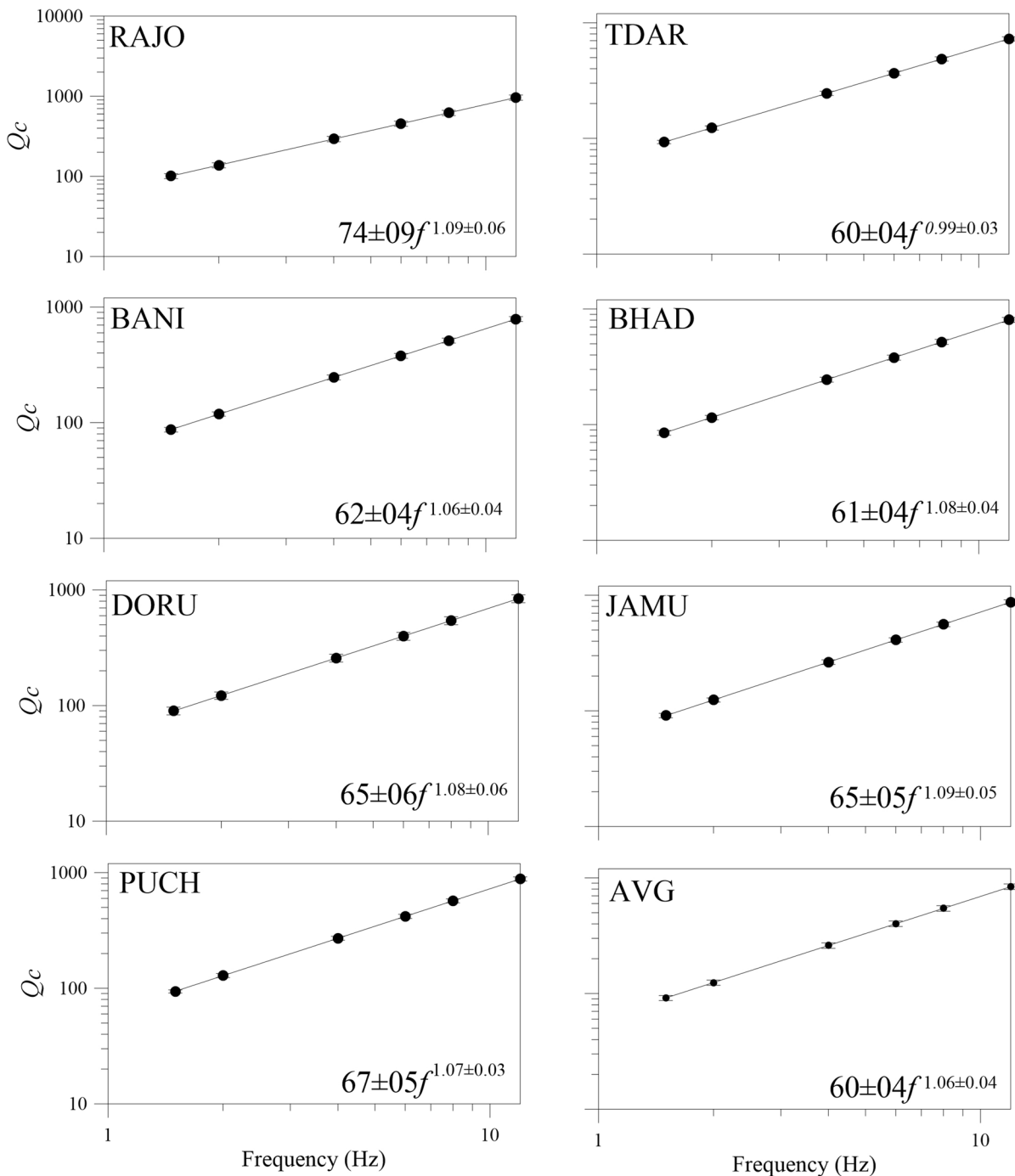
Fig. 3 Power law fit of $Q_c = Q_o f^n$ at individual stations

BHAD station to $(54 \pm 3) f^{(0.68 \pm 0.01)}$ at TDAR station; Q_β varies between $(43 \pm 4) f^{(1.17 \pm 0.02)}$ at BHAD station to $(87 \pm 6) f^{(0.93 \pm 0.04)}$ at PUCH station. Similarly, Q_c varies between $(60 \pm 4) f^{(0.99 \pm 0.03)}$ at TDAR station to $(74 \pm 9) f^{(1.09 \pm 0.06)}$ at RAJO station. The variation of Q_α, Q_β and Q_c at different station suggests varied attenuation characteristics at different locations within the study region. Low Q values are associated

Table 3 Variation of coda Q_c at different frequency band and at three different lapse times

Lapse Time	1.5 Hz $Q_c \pm \sigma$	N	2.0 Hz $Q_c \pm \sigma$	N	4.0 Hz $Q_c \pm \sigma$	N	6.0 Hz $Q_c \pm \sigma$	N	8.0 Hz $Q_c \pm \sigma$	N	12.0 Hz $Q_c \pm \sigma$	N
40	113 ± 42	51	155 ± 65	48	258 ± 90	32	373 ± 110	29	523 ± 122	24	781 ± 141	18
50	114 ± 54	54	158 ± 69	54	266 ± 86	42	399 ± 109	40	513 ± 110	35	758 ± 136	20
60	116 ± 51	44	166 ± 58	47	274 ± 87	43	403 ± 101	37	555 ± 135	30	804 ± 121	12

with higher attenuation and vice versa. Spatial variation of Q at different sites across the study region suggests variation of attenuation properties in the area, which appears to be related to heterogeneities in the local lithological structures and presence of fault(s) beneath the stations (Fig. 1, supplementary Fig. 1; Tables 2, 3, 4, 6 and 7). Stations located on the western part of the study area show higher Q values (low attenuation), in comparison to the eastern part (except at one or two stations). Our analysis suggests that eastern side of the Kishtwar region is more heterogeneous as compared with the western part (Tables 2 and 6). Geological investigations carried out by Thakur (1980) revealed that the Kishtwar and its adjoining area including Ramban, Bhaderwah up to Kashmir consist of meta-sediments of outer crystallines which form the base for the Late Precambrian to Triassic sequence of the Kishtwar and Kashmir basin. The central crystallines of the Zanskar range have been thrust over the Palaeozoic-Mesozoic rocks of the Kishtwar and Kashmir regions. Further, structural analysis revealed that the study area had undergone through three different stages of regional deformation, during which regional and local joints/ faults were developed when the rocks were not in ductile stages (Thakur 1980). Observance of lower seismic wave attenuation beneath Baderwah and Bani stations inferred comparatively the higher level of structural heterogeneity which clearly indicates the presence highly fractured strata or a dense network of joints/ faults in eastern part of the study area (Fig. 1). The occurrence of recent seismicity since 2013 further signifies the reactivation of those faults in this zone of the Kishtwar region.

The lapse-time dependence of coda Q was initially proposed by Rautian and Khalturin (1978) because of the overall decrease of seismic waves attenuation with depth. However, Del Pezzo et al. (2018) pointed out that the increase of Q_c with time may simply reflect the inability of Eq. (1) to capture the full complexity of the scattering process in the Earth. Calvet and Margerin (2013) however, using Monte Carlo simulations of wave transport in a variety of random media demonstrated that the lapse-time dependence of Q_c may also be modeled by multiple anisotropic scattering of seismic waves, without invoking any depth dependence of the attenuation properties in the crust but in this study, we have investigated the lapse time dependence of coda Q_c with depth to study the variation of heterogeneity with depth. The variation of Q_c and Q_o with increasing lapse time windows between 40 and 60 s at an equal interval of 10 s duration shows an increasing trend of Q_c and $Q_o.$ (Tables 3 and 4; Fig. 4). The mean value of coda Q_c varies as $79f^{0.96}$, $80f^{0.89}$ and $83f^{0.88}$ for the lapse time durations of

Table 4 Power las fit $Q_c = Q_o f^n$ for each station at different lapse times

| Lapse Time (S)	BANI $Q_o \pm \sigma$	$n \pm \sigma$	TDAR $Q_o \pm \sigma$	$n \pm \sigma$	RAJO $Q_o \pm \sigma$	$n \pm \sigma$	PUCH $Q_o \pm \sigma$	$n \pm \sigma$
40	76 ± 08	0.87 ± 0.16	83 ± 24	0.90 ± 0.15	71 ± 30	0.89 ± 0.21	64 ± 09	0.93 ± 0.16
50	72 ± 07	0.88 ± 0.17	84 ± 30	0.89 ± 0.18	71 ± 30	0.89 ± 0.21	65 ± 24	0.83 ± 0.21
60	77 ± 11	0.83 ± 0.15	90 ± 20	0.90 ± 0.09	64 ± 05	1.08 ± 0.19	66 ± 04	0.98 ± 0.16
Lapse Time (S)	JAMU $Q_o \pm \sigma$	$n \pm \sigma$	DORU $Q_o \pm \sigma$	$n \pm \sigma$	BHAD $Q_o \pm \sigma$	$n \pm \sigma$	AVG $Q_o \pm \sigma$	$n \pm \sigma$
40	61 ± 05	0.97 ± 0.17	73 ± 09	0.83 ± 0.18	83 ± 14	0.80 ± 0.17	79 ± 05	0.96 ± 0.10
50	66 ± 03	0.98 ± 0.19	68 ± 05	0.96 ± 0.17	80 ± 09	0.96 ± 0.13	80 ± 07	0.89 ± 0.12
60	71 ± 08	0.90 ± 0.15	69 ± 06	0.94 ± 0.18	68 ± 07	0.97 ± 0.15	83 ± 04	0.88 ± 0.10
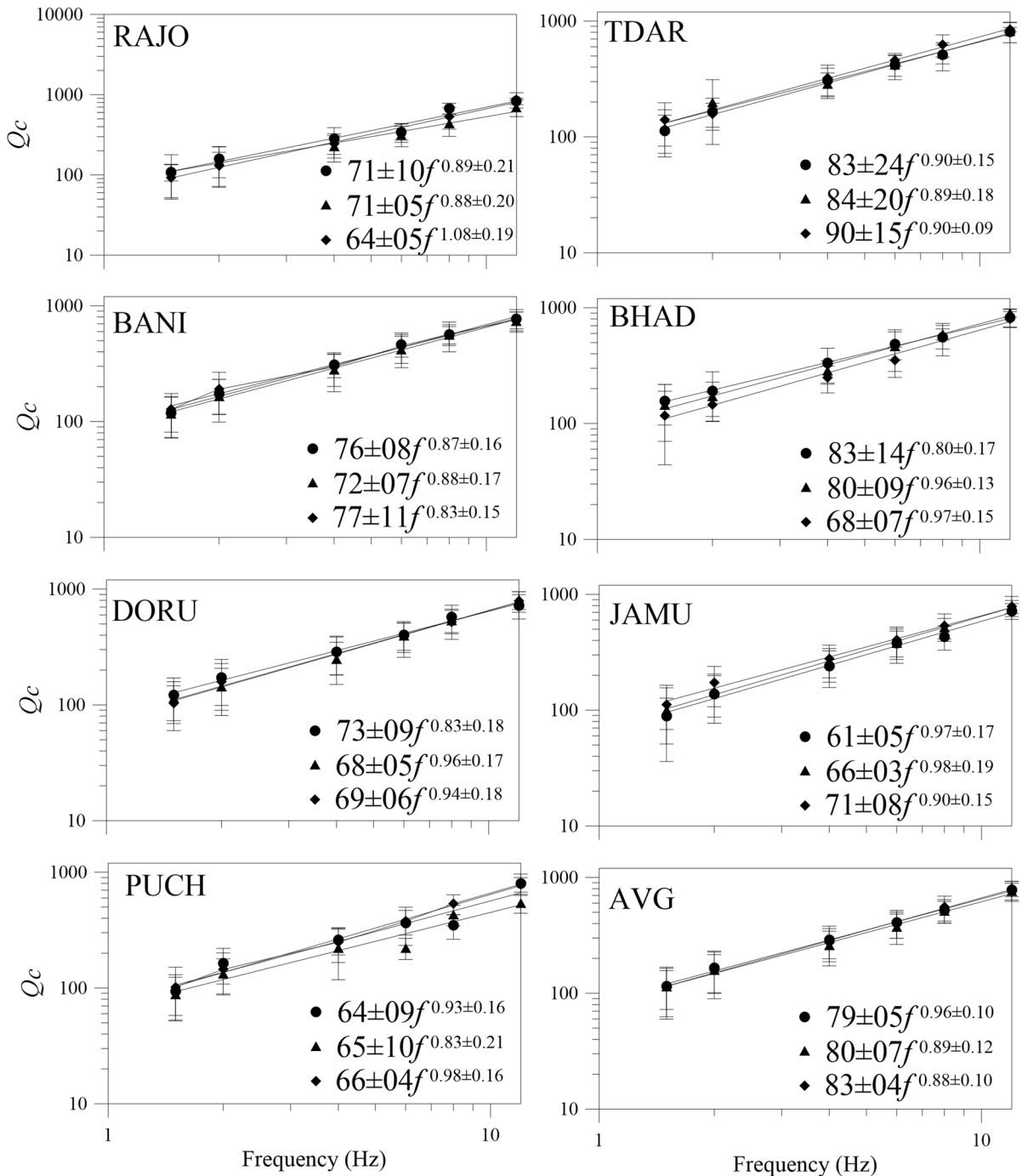
Fig. 4 Q_c variation at individual stations with three different lapse times, circle, triangle and diamond stands for lapse time variation of 40, 50 and 60s, respectively

40, 50 and 60 s, respectively (Fig. 4). The higher Q_o with increasing lapse time indicates that seismic attenuation tends to diminish in the deeper parts of the lithosphere (e.g. Aki & Chouet 1975). At lower frequency, the variation of Q_c and Q_o with increasing lapse time is negligible (Tables 3 and 4) for the

Table 5 Depth estimation of the ellipsoidal volume

Station	Avg. Distance (Δ) in km	Avg. Depth (h_{av}) in km	Avg. Lapse Time (t in s)	a1 = ct/2	$a2 = \sqrt{a1^2 - \Delta^2}$	Depth(km) $h = h_{av} + a2$
JAMU	124.03	10.60	72.40	126.70	25.89	36.49
BANI	86.22	8.97	55.06	96.35	43.01	51.98
DORU	92.51	8.23	56.42	98.73	34.51	42.74
PUCH	82.78	16.22	72.40	126.70	95.92	112.14
RAJO	120.02	12.88	83.05	145.33	81.95	94.84
TDAR	60.66	14.43	54.77	95.84	74.20	88.63
BHAD	81.43	6.81	72.03	126.05	96.21	103.02

Kishtwar region suggesting lower lithosphere to be less heterogeneous for lower frequency, possibly due to the presence of micro-cracks and structural and lithological heterogeneity. The frequency parameter '*n*', which is related to the tectonic activity of the region (Aki 1981; Singh and Herrmann 1983), is found to vary between 0.8 and 1.03 for the study region (Table 4) and suggesting intense seismic activity in the region. It may be seen from Table 5, which lists the estimated ellipsoidal volume for different stations, that the average minimum and maximum focal depths of the events varies from 6.81 to 16.22 km for stations BHAD and PUCH, respectively, while the ellipsoidal depth varies from 37 to 112 km. This is the ellipsoidal volume sampled by coda waves. In the present study, the estimated Qc is assumed to reflect the average

attenuation properties of the ellipsoidal volume containing source and receiver as foci. The spatial extent of the velocity changes caused by coda waves to understand physical mechanisms causing them is studied using the sensitivity kernel (Pacheco and Snieder 2006; Nakahara and Emoto 2017; Del Pezzo et al. 2018), and even in the single scattering model, estimation of the sensitivity kernel is not so simple. Nakahara and Emoto (2017), however, derived an analytical expression of the sensitivity kernels for three-dimensional single-scattering case, which is particularly useful for the analysis of body waves from deeper earthquake. Del Pezzo et al. (2018) on the other hand show that Space weighting functions (SWF) and kernels are different tools that can model the spatial sensitivity of coda envelopes to scattering and absorption anomalies
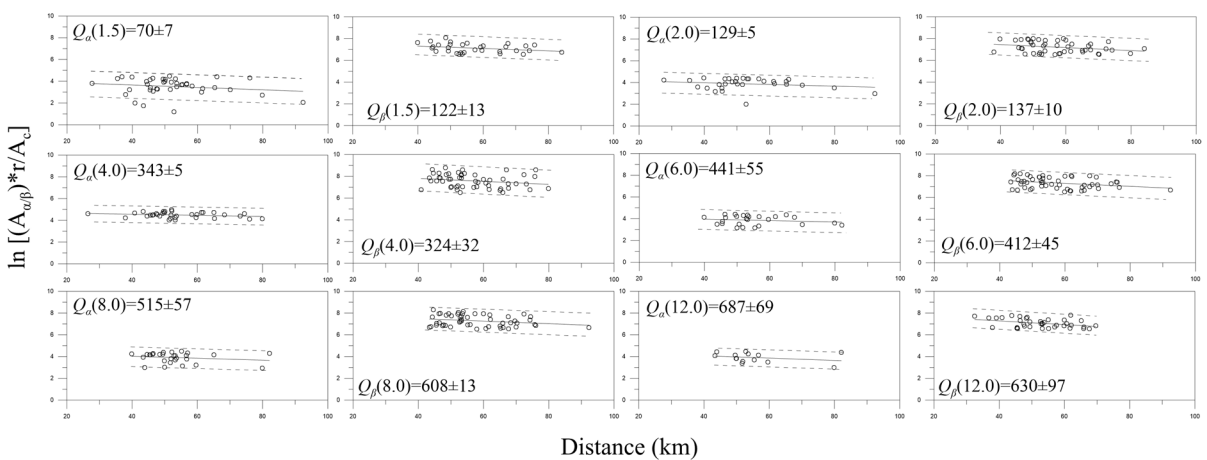

Fig. 5 Decay of coda-normalized peak amplitudes of P- and S-waves with increasing hypocentral distances at six central frequencies for BANI station. The solid line shows the best fitted line using the least-square and the standard deviation of the fit is shown by dotted line

Table 6 Variation of Q_α and Q_β at different frequency band at individual station

Station	BANI		BHAD		DORU		JAMU	
freq	$Q_\alpha \pm \sigma$	$Q_\beta \pm \sigma$	$Q_\alpha \pm \sigma$	$Q_\beta \pm \sigma$	$Q_\alpha \pm \sigma$	$Q_\beta \pm \sigma$	$Q_\alpha \pm \sigma$	$Q_\beta \pm \sigma$
1.5	70 ± 7	122 ± 13	33 ± 5	88 ± 5	71 ± 3	89 ± 10	86 ± 16	67 ± 12
2	129 ± 5	137 ± 10	69 ± 2	89 ± 2	124 ± 13	99 ± 5	69 ± 8	89 ± 4
4	343 ± 5	324 ± 32	86 ± 6	162 ± 6	250 ± 47	198 ± 8	147 ± 10	119 ± 17
6	441 ± 55	412 ± 55	140 ± 11	412 ± 11	484 ± 50	282 ± 25	154 ± 31	382 ± 25
8	515 ± 57	608 ± 13	186 ± 20	357 ± 20	593 ± 93	397 ± 9	242 ± 15	357 ± 17
12	687 ± 69	630 ± 94	229 ± 78	1071 ± 80	1030 ± 90	535 ± 25	562 ± 5	119 ± 6
Station	PUCH		RAJO		TDAR		Average	
freq	$Q_\alpha \pm \sigma$	$Q_\beta \pm \sigma$	$Q_\alpha \pm \sigma$	$Q_\beta \pm \sigma$	$Q_\alpha \pm \sigma$	$Q_\beta \pm \sigma$	$Q_\alpha \pm \sigma$	$Q_\beta \pm \sigma$
1.5	64 ± 5	112 ± 2	97 ± 19	134 ± 15	63 ± 4	134 ± 13	69 ± 9	106 ± 13
2	86 ± 17	223 ± 25	129 ± 12	149 ± 5	79 ± 14	162 ± 16	98 ± 10	135 ± 9
4	257 ± 2	357 ± 38	250 ± 69	510 ± 84	204 ± 2	178 ± 9	220 ± 20	264 ± 28
6	238 ± 32	268 ± 62	515 ± 74	268 ± 14	158 ± 3	357 ± 25	304 ± 36	340 ± 31
8	187 ± 8	714 ± 65	1373 ± 44	476 ± 56	277 ± 40	714 ± 45	482 ± 40	517 ± 32
12	515 ± 2	1071 ± 97	2060 ± 187	1338 ± 149	230 ± 17	1071 ± 95	759 ± 64	834 ± 78

in these rock matrices and reported that Q_c is not a physical parameter of the propagation medium; it is even more efficient as a velocity independent imaging tool for magma and fluid storage when applied to deep volcanism. Similarly, Pacheco and Snieder (2006) calculated the mean travel time change for any given source-receiver pair due to localized perturbation in the propagation velocity, which can be used in evaluation of heterogeneous materials and monitoring of time-lapse heterogeneous reservoirs.

Further analysis suggests, $Q_\beta > Q_\alpha$ (varies between 1.2 and 1.5) for the entire frequency ranges (Tables 6 and 7), suggesting that P-waves attenuate faster compared with S-waves. Variations in Q_α and Q_β at different locations in the Kistwar region may be attributed to porosity, temperature variations, grain boundary sliding, presence of fluids

and heterogeneity in local lithology (Hauksson and Shearer 2006).

It is well established that Intrinsic and scattering mechanisms are mainly responsible for attenuation of seismic waves in the lithosphere. The intrinsic mechanism is mainly caused due to the presence of small-scale crystal dislocations, frictional heating and movement of fluids present in the porous medium, in contrast to the scattering attenuation which deals with the loss of energy of a direct wave caused by reflection, refraction and conversion (Sato 1984). Verma et al. (2015) reported the role of fluids in the earthquake genesis of Kangra and its surrounding areas, which is also a prominent factor in seismic wave attenuation and can be inferred from the study of attenuation quality factors. Based on a laboratory experiment using ultrasonic

Table 7 Power las fit $Q = Q_o f^n$ for each station

| #	Station code	$Q_\alpha = (Q_o \pm \sigma) f^{(n+SD)}$	$Q_\beta = (Q_o \pm \sigma) f^{(n+SD)}$	$Q_c = (Q_o \pm \sigma) f^{(n+SD)}$
1	BANI	$56 \pm 7 f^{1.00 \pm 0.1}$	$83 \pm 3 f^{0.87 \pm 0.01}$	$62 \pm 4 f^{1.06 \pm 0.04}$
2	BHAD	$28 \pm 2 f^{0.86 \pm 0.08}$	$43 \pm 4 f^{1.17 \pm 0.02}$	$61 \pm 4 f^{1.08 \pm 0.04}$
3	DORU	$45 \pm 4 f^{1.23 \pm 0.02}$	$57 \pm 5 f^{0.9 \pm 0.02}$	$65 \pm 6 f^{1.08 \pm 0.06}$
4	JAMU	$45 \pm 9 f^{0.87 \pm 0.09}$	$64 \pm 9 f^{0.57 \pm 0.06}$	$65 \pm 5 f^{1.09 \pm 0.05}$
5	PUCH	$50 \pm 9 f^{0.87 \pm 0.06}$	$87 \pm 6 f^{0.93 \pm 0.04}$	$67 \pm 5 f^{1.07 \pm 0.03}$
6	RAJO	$32 \pm 3 f^{1.5 \pm 0.11}$	$83 \pm 3 f^{0.96 \pm 0.02}$	$74 \pm 9 f^{1.09 \pm 0.06}$
7	TDAR	$54 \pm 3 f^{0.68 \pm 0.01}$	$79 \pm 10 f^{1.00 \pm 0.02}$	$60 \pm 4 f^{0.99 \pm 0.03}$
	Average	$44 \pm 6 f^{1.01 \pm 0.91}$	$71 \pm 6 f^{0.91 \pm 0.01}$	$60 \pm 6 f^{1.06 \pm 0.04}$
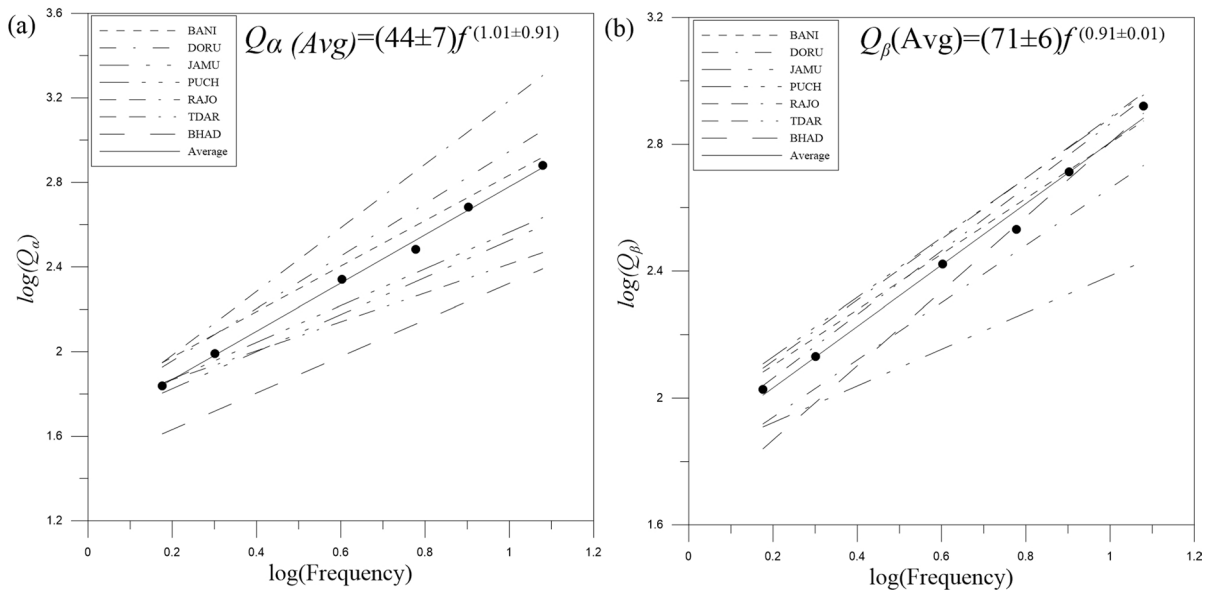
Fig. 6 (**a**) and (**b**) shows the power law fit for $Q_\alpha = Q_o f^n$ and $Q_\beta = Q_o f^n$, respectively, at individual stations, and the average value is plotted by solid line

frequency Toksoz et al. (1979) demonstrated that fluid saturation plays a key role in controlling quality factor Q within the seismogenic crust. According to their report, Q_α is 10–25% larger than Q_β in fully saturated (in fluid) rocks, whereas, $Q_\alpha < Q_\beta$ in
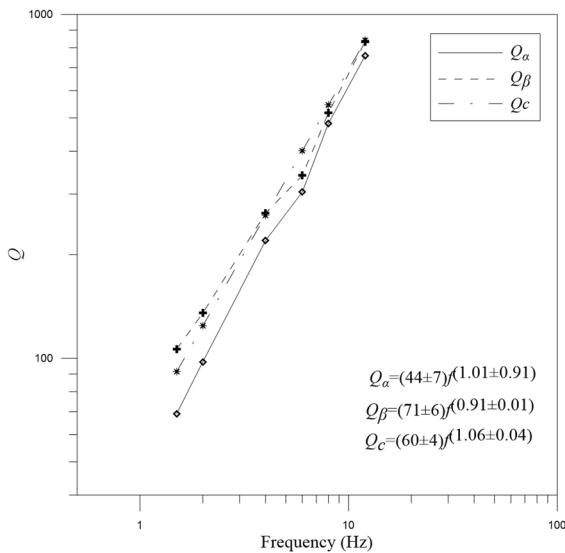

Fig. 7 Comparative plot of the average value of the power law fit of $Q_c = Q_o f^n$, $Q_\alpha = Q_o f^n$ and $Q_\beta = Q_o f^n$ of the study area

partially saturated rocks, at both low and high pressures, and the relative fluid saturation may influence the spatial distribution of Q_β/Q_α ratio. Sites, having $Q_\beta/Q_\alpha > 1$ may be the regions, where the dominating mechanism of seismic wave attenuation must be scattering, due to the presence of different heterogeneity in the crust. The other interpretation could be based on the fact that both P- and S-waves suffer similar intrinsic attenuation, while P-waves suffer more attenuation due to scattering effect (Hauksson and Shearer 2006). We affirm here that the observed high value of Q_β/Q_α (> 1) in the study area, except for RAJO and DARO, for the Kishtwar region (Table 6; Fig. 7), maybe due to scattering from shallow heterogeneities in the study area. The higher Q_β/Q_α, i.e. > 1, as observed for the Kishtwar region (Table 6; Fig. 7) has also been reported for many other regions in the world and these values are structurally correlated with a high degree of lateral heterogeneity in the upper crust (Singh et al. 2012; Sato and Fehler 1998). The presence of high degree of heterogeneity in the upper crust is attributed to the presence of faults, lineaments and micro-cracks in the rock types. Furthermore, the Kishtwar region is located close to the collision boundary between Indian and Eurasian plates, which also suggests the presence of a high degree of heterogeneity in the
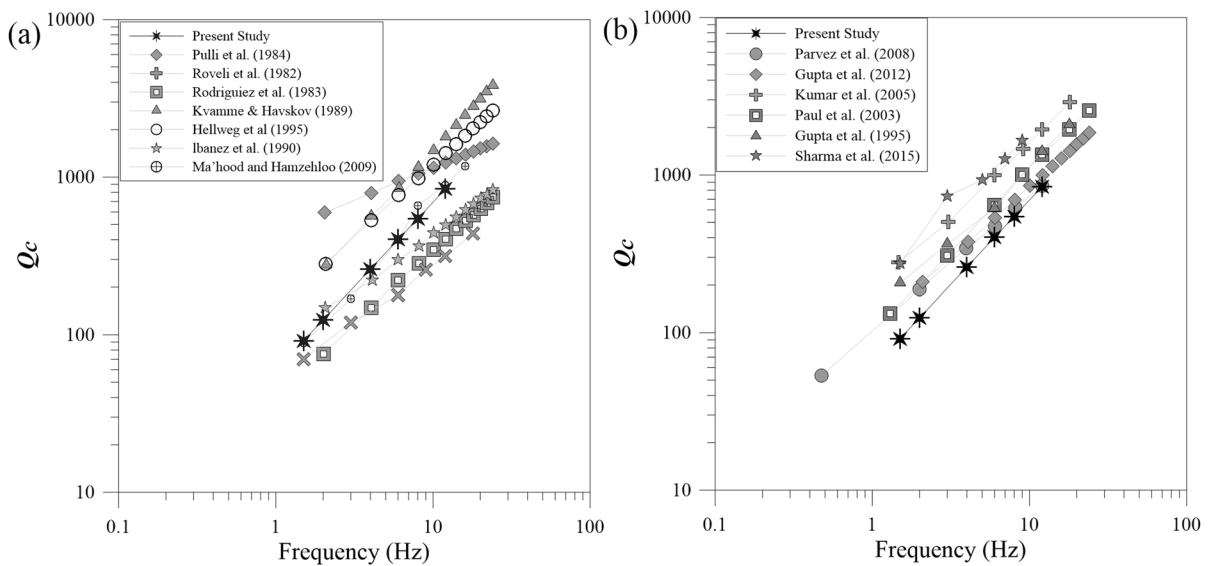
Fig. 8 Comparison of estimated coda Q (Q_c) of the study area with (**a**) different regions across the world and (**b**) in India

upper crust. Also, local faults and thrusts, mostly the splays of major continental NW–SE trending faults/thrust, such as MBT, MCT, JT and PT, play an important role in controlling the attenuation characteristics of the region.

The estimated coda attenuation quality factor (Q_c) of the study area is well comparable to that of Andaman region in India and East-central Iran (Fig. 8). The major cause of seismicity in Andaman region is the subduction of the Indian oceanic plate beneath the Sunda plate. Geologically, this region is exposed to pre-Cretaceous meta-sedimentary rocks, upper Cretaceous ophiolites and Palaeogene-Neogene sedimentary formations (Bandopadhyay and Carter 2017). Similarly, East-Central Iran is part of the Alpine-Himalayan orogenic belt that resulted due to continent–continent collision between Arabian and Eurasian plates and has similar tectonic setup as that of the Himalaya, which forms due to collision between India and Eurasian plates. Geologically, the East-Central Iran consisted of mixed sedimentary, intermediate, felsic igneous rocks (Mahmood et al. 2009a), which are similar to the study area. The lithological succession of the Kishtwar region comprises of metamorphites (Proterozoic) unconformably overlain by Palaeozoic-Mesozoic Tethyan sediments and appears to be tectonically and geologically similar to above-said regions.

Q_β estimates of Kishtwar region are closer to that of the northeast region of India and east-central Iran (Fig. 9). It may be noted that northeast India is one of the seismically very active regions of India and lies at the junction of the Himalaya and Burmese arc. The earthquakes in these regions are related to collision as well as subduction tectonics and are correlated with the regional mega thrust like MBT and MCT, which are also running across the Kishtwar region. Q_α, on the other hand, found comparable to northeast India for the higher frequency part, whereas in the lower frequency it is comparable to East Central Iran, which is situated in an active collision zone.

6 Conclusions

Considering the seismically active nature of Kishtwar area of Kashmir seismic gap in NW Himalaya, we have carried out first seismic attenuation study of Kishtwar region using P-, S- and coda waves of 161 earthquakes recorded by a local network of 7 BBS stations. The attenuation quality factors, Q_α, Q_β and Q_c, are found to be strongly dependent on frequency and increase with the increasing central frequency. Most of the sites having higher Q are located on the western side of the study area and suggest that the western part of the Kishtwar region is more
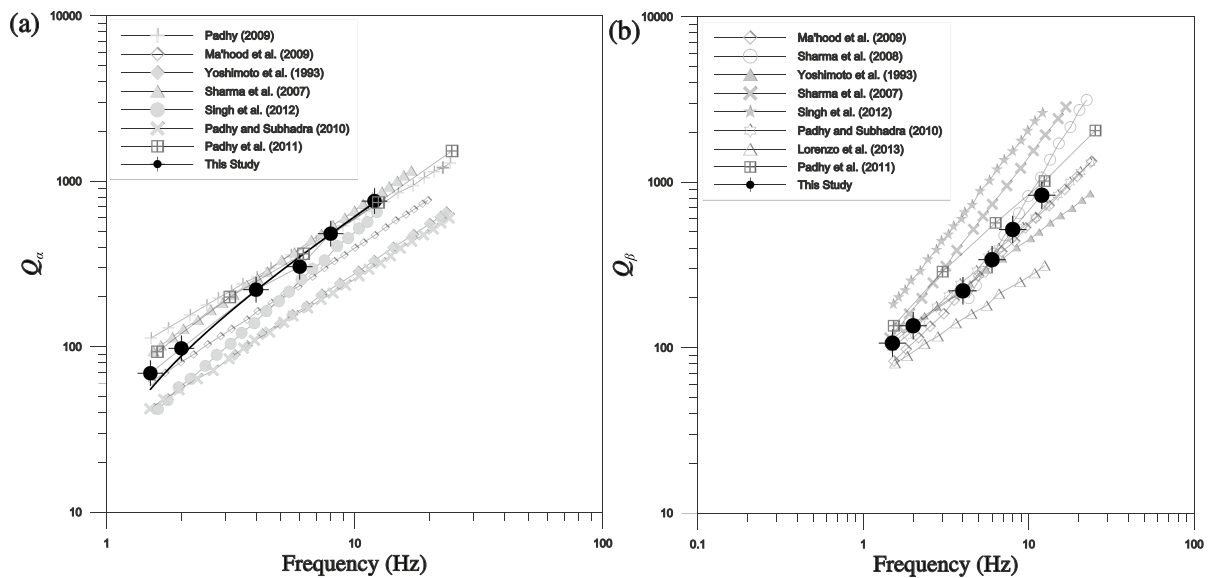
Fig. 9 Comparison of the estimated attenuation quality factors (**a**) Q_α and (**b**) Q_β of the study area with different regions across India and around the world

homogenous compared with the Eastern part. The variation of Q_c with increasing lapse time suggests that the upper crust is more heterogenous as compared with the lower lithosphere, possibly due to the presence of numerous micro-cracks and structural deformation. Analysis of the quality factors of P and S waves shows that average Q_β of the Kishtwar region is higher compared to Q_α, for the entire frequency range (1.5–12 Hz), which implies that P-waves suffers more attenuation compared with the S-waves. The dominant mechanism of attenuation in the Kishtwar region is found to be scattering in the crust. The estimated quality factors are found comparable with other tectonically active regions of the world, having similar geology and tectonics as that of the Kishtwar region. The results of the study will be useful in constraining the earthquake source parameters, hazard assessment and strong ground motion simulation.

References

Aki K (1969) Analysis of the seismic coda of local earthquakes as scattered waves. J Geophys Res 74(2):615–631. https://doi.org/10.1029/jb074i002p00615

Aki K (1981) Scattering and attenuation of high-frequency body waves (1–25 Hz) in the lithosphere. Phys Earth Planet Inter 26(4):241–243. https://doi.org/10.1016/0031-9201(81)90026-1

Aki K, Chouet B (1975) Origin of coda waves: Source, attenuation, and scattering effects. J Geophys Res 80(23):3322–3342. https://doi.org/10.1029/JB080i023p03322

Bandopadhyay PC, Carter A (2017) The Andaman – Nicobar Accretionary Ridge: Geology. Tectonics and Hazards. Geol Soc Lond 47:237

Calvet M, Margerin L (2013) Lapse-time dependence of coda Q: Anisotropic multiple-scattering models and application to the Pyrenees. Bull Seism Soc Am 103:1993–2010. https://doi.org/10.1785/0120120239

Del Pezzo E, De La Torre A, Bianco F, Ibanez J, Gabrielli S, De Siena L (2018) Numerically calculated 3D space-weighting functions to image crustal volcanic structures using diffuse coda waves. Geosciences 8:175. https://doi.org/10.3390/geosciences8050175

Gupta SC, Singh VN, Kumar A (1995) Attenuation of coda waves in the Garhwal Himalaya, India. Phys Earth Planet Inter 87(3–4):247–253. https://doi.org/10.1016/0031-9201(94)02968-H

Gupta AK, Sutar AK, Chopra S, Kumar S, Rastogi BK (2012) Attenuation characteristics of coda waves in Mainland Gujarat (India). Tectonophysics 530–531:264–271. https://doi.org/10.1016/j.tecto.2012.01.002

Hauksson E, and Shearer PM (2006) Attenuation models (Q_P and Q_S) in three dimensions of the southern California crust: Inferred fluid saturation at seismogenic depths. J Geophys Res 111:B05302. https://doi.org/10.1029/2005JB003947

Havskov J, Ottemöller L (2010) Routine data processing in earthquake seismology: with sample data, exercises and software. Springer. https://doi.org/10.1007/978-90-481-8697-6

Hellweg M, Spudich P, Fletcher JB, Baker LM (1995) Stability of coda Q in the region of Parkfield, California: View from the U.S. Geological Survey Parkfield Dense Seismograph Array. J Geophys Res: Solid Earth 100(B2):2089–2102. https://doi.org/10.1029/94JB02888

Ibáñez JM, Pezzo ED, De Miguel F, Herriaz M, Alguacie G, Morales J (1990) Depth dependent seismic attenuation in the Granada zone (Southern Spain). Bull Seismol Soc Am 80:1232–1244

Kvamme LB, Havskov J (1989) Q in Southern Norway. Bull Seismol Soc Am 79:1575–1588

Knopoff L (1964) Q. Rev Geophys 2(4):625. https://doi.org/10.1029/RG002i004p00625

Kumar N, Parvez IA, Virk HS (2005) Estimation of coda wave attenuation for NW Himalayan region using local earthquakes. Phys Earth Planet Inter 151(3–4):243–258. https://doi.org/10.1016/j.pepi.2005.03.010

Kumar N, Sharma J, Arora BR, Mukhopadhyay S (2009) Seismotectonic model of the Kangra-Chamba sector of Northwest Himalaya: Constraints from joint hypocenter determination and focal mechanism. Bull Seismol Soc Am 99(1):95–109. https://doi.org/10.1785/0120080220

Lorenzo SD, Edoardo DP, Francesca B (2013) Qc, Qβ, Qi and Qs attenuation parameters in the Umbria–Marche (Italy) region. Phys Earth Planet Inter 218:19–30. https://doi.org/10.1016/j.pepi.2013.03.002

Ma'hood M, Hamzehloo H (2009) Estimation of coda wave attenuation in East Central Iran. J Seismol 13: 125–139. https://doi.org/10.1007/s10950-008-9130-2

Ma'hood M, Hamzehloo H, Doloei GJ, (2009) Attenuation of high frequency *P* and *S* waves in the crust of the East-Central Iran. Geophys J Int 179(3):1669–1678. https://doi.org/10.1111/j.1365-246X.2009.04363.x

Mitchell BJ (1995) Anelastic structure and evolution of the continental crust and upper mantle from seismic surface wave attenuation. Reviews of Geophysics 33:441–462

Nakahara H, Emoto K (2017) Deriving sensitivity kernels of coda-wave travel time to velocity changes based on the tree-dimensional single isotropic scattering model, Pure Appl. Geophys 174:327–337. https://doi.org/10.1007/s00024-016-1358-0

Pacheco C, Snieder R (2006) Time-lapse travel time change of singly scattered acoustic waves. Geophys J Int 165:485–500. https://doi.org/10.1111/j.1365-246X.2006.02856.x

Padhy S, Subhadra N (2010) Attenuation of high-frequency seismic waves in northeast India. Geophys J Int 181:453–467

Padhy S, Subhadra N, Kayal JR (2011) Frequency-dependent attenuation of body and coda waves in the Andaman Sea Basin. Bull Seismol Soc Am 101(1):109–125. https://doi.org/10.1785/0120100032

Padhy S (2009) Characteristics of body wave attenuations in the Bhuj crust. Bull Seismol Soc Am 99:3300–3313

Pandey SJ, Bhat GM, Puri S, Raina N, Singh Y, Pandita SK, Verma M, Bansal BK, Sutar AK (2016) Seismotectonic study of Kishtwar region of Jammu Province using local broadband seismic data. Journal of Seismology 21(3):525–538

Parvez IA, Sutar AK, Mridula M, Mishra SK, Rai SS (2008) Coda Q Estimates in the Andaman Islands Using Local Earthquakes. Pure Appl Geophys 16:1861–1878

Pulli JJ (1984) Attenuation of coda waves in New England. Bull Seismol Soc Am 74(4):1149–1166

Paul A, Gupta SC, Pant CC (2003) CODA Q estimates for Kumaun Himalaya. J Earth Syst Sci 112:569–576. https://doi.org/10.1007/BF02709780

Peng JY, Aki K, Chouet B, Johnson P, Lee WHK, Marks S, Tottingham DM (1987) Temporal change in coda associated with the Round Valley, California, Earthquake of November 23, 1984. J Geophys Res 92(B5):3507. https://doi.org/10.1029/JB092iB05p03507

Rautian TG, Khalturin VI (1978) The use of the coda for determination of the earthquake source spectrum. Bull Seismol Soc Am 68:923–948

Rovelli A (1982) On the frequency dependence of Q in Friuli from short-period digital records. Bull Seismol Soc Am 72(6A):2369–2372

Rodriguez M, Havskov J, Singh SK (1983) Q from Coda Waves near Petatlan, Guerrero, Mexico. Bull Seismol Soc Am 73:321–326

Sato H (1984) Attenuation and envelope formation of three-component seismograms of small local earthquakes in randomly inhomogeneous lithosphere. J Geophys Res 89:1221–1241

Sato H, Fehler M (1998) Scattering and Attenuation of Seismic Waves in Heterogeneous Earth. AIP Press, Springer Verlag, New York

Sharma B, Teotia SS, Kumar D (2007) Attenuation of P, S, and coda waves in Koyna region, India. J Seismol 11:327–334

Sharma B, Gupta AK, Devi DK, Kumar D, Teotia SS, Rastogi BK (2008) Attenuation of high-frequency seismic waves in Kachchh region, Gujarat, India. Bull Seismol Soc Am 98(5):2325–2340

Sharma B, Chingtham P, Sutar AK, Chopra S, Shukla HP (2015) Frequency dependent attenuation of seismic waves for Delhi and surrounding area. India Ann Geophys 58(2):S0216

Singh C, Srinivasa Bharathi VK, Chadha RK (2012) Lapse time and frequency-dependent attenuation characteristics of Kumaun Himalaya. J Asian Earth Sci 54:64–71

Singh S, Herrmann RB (1983) Regionalization of crustal coda Q in the continental United States. J Geophys Res 88(B1):527. https://doi.org/10.1029/JB088iB01p00527

Stein S, Wysession M (2003) Introduction to Seismology, Earthquakes, and Earth Structure. Blackwell Publishing

Thakur VC (1980) Tectonics of the Central Crystallines of western Himalaya. Tectonophysics 62(1–2):141–154. https://doi.org/10.1016/0040-1951(80)90142-0

Thakur VC (1992) Geology of Western Himalaya. Pergamon

Toksoz MN, Johnston AH, Timur A (1979) Attenuation of seismic waves in dry and saturated rocks. I Laboratory Measurements. Geophys 44:681–690

Valdiya KS (2016) The Making of India Geodynamic Evolution, 2nd edn. Springer International Publishing, Switzerland

Verma M, Sutar AK, Bansal BK, Arora BR, Bhat GM (2015) M_W 4.9 earthquake of 21August, 2014 in Kangra region, Northwest Himalaya: Seismotectonics implications. J Asian Earth Sci 109:29–37. https://doi.org/10.1016/j.jseaes.2015.05.006

Wadia DN (1931) The syntaxis *of* Northwest Himalaya*: Its Rocks,* Tectonics and Orogeny. Rec Geol Surv India 65:189–220

Yoshimoto K, Sato H, Ohtake M (1993) Frequency-dependent attenuation of P and S waves in the Kanto area, Japan, based on the coda normalization method. Geophys J Int 114(1):165–174

Publisher's note Springer Nature remains neutral with regard to jurisdictional claims in published maps and institutional affiliations.